Climate-Regulation of Organic Carbon Export in Erosive Mountain Settings: A Case Study from Taiwan since the Last Glacial Maximum

Li-Wei Zheng[1,2*], Robert G. Hilton[3], Yuan-Pin Chang[4], Rick J. Yang[4], Xiaodong Ding[5], Xufeng Zheng[1,2], Tsung-Yu Lee[6], Hsi-Jih Lu[4], Jung-Tai Lu[4], Yu-Shih Lin[4], James T. Liu[4], Shuh-Ji Kao[2*]

[1] School of Marine Science and Engineering, Hainan University, Hainan, China

[2] State Key Laboratory of Marine Resource Utilization in South China Sea, Hainan University, Hainan, China..

[3] Department of Earth Sciences, University of Oxford, South Parks Road, Oxford, UK

[4] Department of Oceanography, National Sun Yat-sen University, Kaohsiung, Taiwan, ROC.

[5] College of Biological Science & Engineering, North Minzu University, Yinchuan, China.

[6] Department of Geography, National Taiwan Normal University, Taipei, Taiwan, ROC.

Corresponding author: Li-Wei Zheng (zlw@hainanu.edu.cn);

Shuh-Ji Kao (sjkao@xmu.edu.cn);

Abstract

The balance between the burial of biospheric organic carbon (OC_{bio}) in the ocean and the oxidation of rock-derived organic carbon across landscapes (OC_{petro}) helps to regulate atmospheric CO_2 and O_2 over geological time. However, we lack reconstructions of these processes over the timescales necessary to properly understand the drivers and feedbacks operating. Here we use a sediment core from the Zhuoshui River delta in Taiwan, which receives sediments from a rapidly uplifting and eroding catchment, to reconstruct the variations in OC content and radiocarbon composition since the Last Glacial Maximum (LGM). We find that the export of OC_{bio} and the oxidation of OC_{petro} are both modulated by climate-driven changes in physical erosion and temperature. During cold and dry periods, such as the LGM and the Younger Dryas (YD), shallow erosion and low temperature enhanced the preservation of OC_{bio} in the biosphere in catchment, while deep erosion and high temperature during warm and wet periods, such as the Holocene, favored the dilution and degradation of OC_{bio}. The weathering intensity of OC_{petro} (ω) was inversely related to physical erosion, suggesting a lower intensity of oxidation during the Holocene period while the overall oxidation flux was enhanced. This suggests that the degree of weathering was primarily controlled by physical erosion. We propose a proxy to estimate the ratio of fluxes of OC_{bio} export and OC_{petro} oxidation, and show that the net balance between these two processes shifted from a carbon sink during the late deglacial period to a carbon source during the mid-late Holocene. Our study reveals that with CO_2 rise, a warmer and wetter climate would promote the exposure and oxidation of OC_{petro} by erosion in this mountain range, leading the organic carbon balance towards a CO2 source to the atmosphere.

1 Introduction

The amount of organic carbon (OC) stored in rocks, soil, and vegetation are orders of magnitude higher than the stock of carbon in the atmosphere (Sundquist and Visser, 2004), thus, the atmospheric carbon inventory is sensitive to small imbalances between these large reservoirs. The erosion of the continents and accompanied export of particulate organic carbon (POC) by rivers from land to the ocean is an important component of global carbon cycle (Sarmiento and Sundquist, 1992; Stallard, 1998; Galy et al., 2015). The particulate OC exported by rivers can be conceptualized as a mixture of recently photosynthesized, biospheric carbon (OC_{bio}) from plants and soils (Kao and Liu, 1996; Hilton et al., 2008); and rock–derived, or petrogenic OC (OC_{petro}) from sedimentary rocks.

From the perspective of the global carbon balance prior to anthropogenic perturbation, the OC_{bio} exported from continents by rivers (0.11 - 0.23 Pg yr^{-1}, Galy et al., 2015) is comparable to the amount of OC burial in marine sediments (0.2 Pg yr^{-1}, Hedges and Keil, 1995). Yet, the overall transfer by rivers and (re-) burial of OC_{petro} is disconnected from the atmosphere having no impact on atmospheric CO_2 (Galy et al., 2008), unless the oxidation of OC_{petro} in the landscape occurs during its exhumation, releasing carbon dioxide (Bouchez et al., 2010; Hilton et al., 2014; Hemingway et al., 2018; Blattmann, 2018; Lyons et al., 2018; Horan et al., 2017, 2019). Over geological timescales, atmospheric carbon dioxide and oxygen concentrations are, in part, regulated by the relative fluxes of OC_{petro} oxidation and sedimentary burial of OC_{bio} from terrestrial biosphere (Berner, 1982; Galy et al., 2008; Lyons et al., 2018; Horan et al., 2019; Derry and France-Lanord, 1996). Understanding the factors that control the export of OC_{bio} and OC_{petro} during transfer is therefore crucial.

Physical erosion plays a crucial role in controlling the riverine export of both OC_{bio} and OC_{petro} to the oceans on a global scale (Galy et al., 2015, Hilton, 2016). However, the oxidation of OC_{petro} may be supply-limited and able to keep pace with increasing physical erosion (Hilton et al., 2014, Hemingway et al., 2018). As atmospheric CO_2 concentrations continue to rise, warmer and more humid climate condition are expected (O'Gorman et al., 2012) which may promote physical erosion rates in some settings (Lee et al., 2015). However, the extent to which climate change may tilt the balance between the export of OC_{bio} and the oxidation of OC_{petro} in erosive settings remains poorly constrained (Hilton and West, 2020).

Globally, temperature and precipitation exert primary control on the residence time of OC_{bio} within river catchments (Eglinton and Galy, 2021). The Ganges–Brahmaputra basin illustrates this dynamic on millennial timescales, where the residence time of soil carbon decreased across the deglaciation period due to increased rainfall and enhanced soil respiration rates (Hein et al., 2020). Similarly, the oxidation of OC_{petro} in river catchments is also found to be temperature-dependent (Roylands et al., 2022; Soulet et al., 2021), underscoring the significant influence of climatic factors on weathering processes. Examining the records across periods of significant climatic shifts, such as the last deglaciation, can help us better understand the relationship between climate change and the carbon cycle.

Taiwan, a mountainous subtropic island located in an orogenic belt with rapid uplift and denudation rates (3-6 mm yr^{-1}, Dadson et al., 2003), provides an opportunity to study the evolution of OC_{bio} and OC_{petro} export. Palynological and sedimentary organic geochemistry evidence has suggested the climate in Taiwan was influenced by the variation in the strength of the East Asian summer monsoon (EASM). During the Last Glacial Maximum (LGM, 22 - 18 cal ka BP) and the

deglaciation (18 - 11.6cal ka BP), the climate was cold and dry, while during the Holocene to the present day the climate was humid and warm (e.g. Liew et al., 1998, 2006; Yang et al., 2011, Ding et al., 2016a, 2020). In addition to the strengthening of the EASM from the LGM to the Holocene, the frequency of tropical cyclones (typhoons) had also increased, evidenced by records of ancient landslides (Hsieh et al., 2012, 2014), sea spray signal in lake sediments (Ding et al., 2016b), and turbitide layers in marine sediment cores offshore of Taiwan (Yu et al., 2017). Collectively, the geomorphic setting and climatic change experienced by Taiwan provide a case to shed new light on how the net carbon balances during erosion and weathering may have changed over millennial timescales. To achieve this goal, it is necessary to track the erosion and export of OC_{bio} and OC_{petro} (Kao et al., 2008), while also being able to assess OC_{petro} oxidation in the past, which to date has proved challenging.

Here we address these issues by synthesizing and re-analyzing modern field-based observations from the mountains of Taiwan (e.g. Hilton et al., 2010, 2011, 2012, 2014; Kao et al., 2014; Hemingway et al., 2018) to address the impact of physical erosion, temperature effects on OC content (including OC_{bio} and OC_{petro}) and its ^{14}C activity in soil and river suspended particles, and extrapolate these relationships to the past. We then assess changes in the erosion and delivery of OC_{bio} and OC_{petro} during the last deglaciation by using a sediment core in a river delta receiving sediments from the Central Range, Taiwan. Using radiocarbon to establish the difference between the timing of sediment deposition (determined from calcareous microfossils and woody debris) and the ^{14}C of the bulk OC, we explore variations in the sedimentary burial of OC_{petro} and OC_{bio} over time. Linking the modern and sedimentary datasets, we propose a new proxy to quantify past variations in the relative rates of OC_{bio} export and OC_{petro} oxidation, and assess the net CO_2 balance during erosion of a mountain range since the last deglaciation.

2 Materials and Methods

2.1 Study area and sampling

The collision of the Eurasia and Philippine Sea Plate drives the uplift of Taiwan since approximately 6 million years ago (Ma), with a denudation rate of ~ 3-6 mm yr^{-1} (Dadson et al., 2003). The Zhuoshui (also referred to the Jhoushui and Choshui River due to different Romanization schemes) River drains the western flank of the Central Range of Taiwan. The bedrock in the river basin consists of Miocene and Pliocene metasedimentary, low-grade metamorphic, and sedimentary rocks (Ho, 1988) (Figure 1). The frequent impact of tropical cyclones delivers intense precipitation, and this combines with the high uplift rates to drive remarkably high sediment yields (Dadson et al., 2003; Kao and Milliman, 2008) where rivers often carry suspended sediments at hyperpycnal concentrations (turbidity > 40g L^{-1}) (Goldsmith et al., 2008). The Zhuoshui River is the largest river in Taiwan in terms of sediment discharge (Kao and Milliman, 2008). Such high turbidity results in rapid accumulation of sediment offshore, reducing the oxygen exposure time of organic matter (Blair and Aller, 2012). As such, the preservation efficiency of riverine OC is > 80% (Kao et al., 2014), which is higher than the global average (20-

30%, Burdige, 2005). Therefore, the OC preserved in the offshore sediments might reflect the erosion dynamic in the river catchment with limited influence by the post-diagenesis processes.

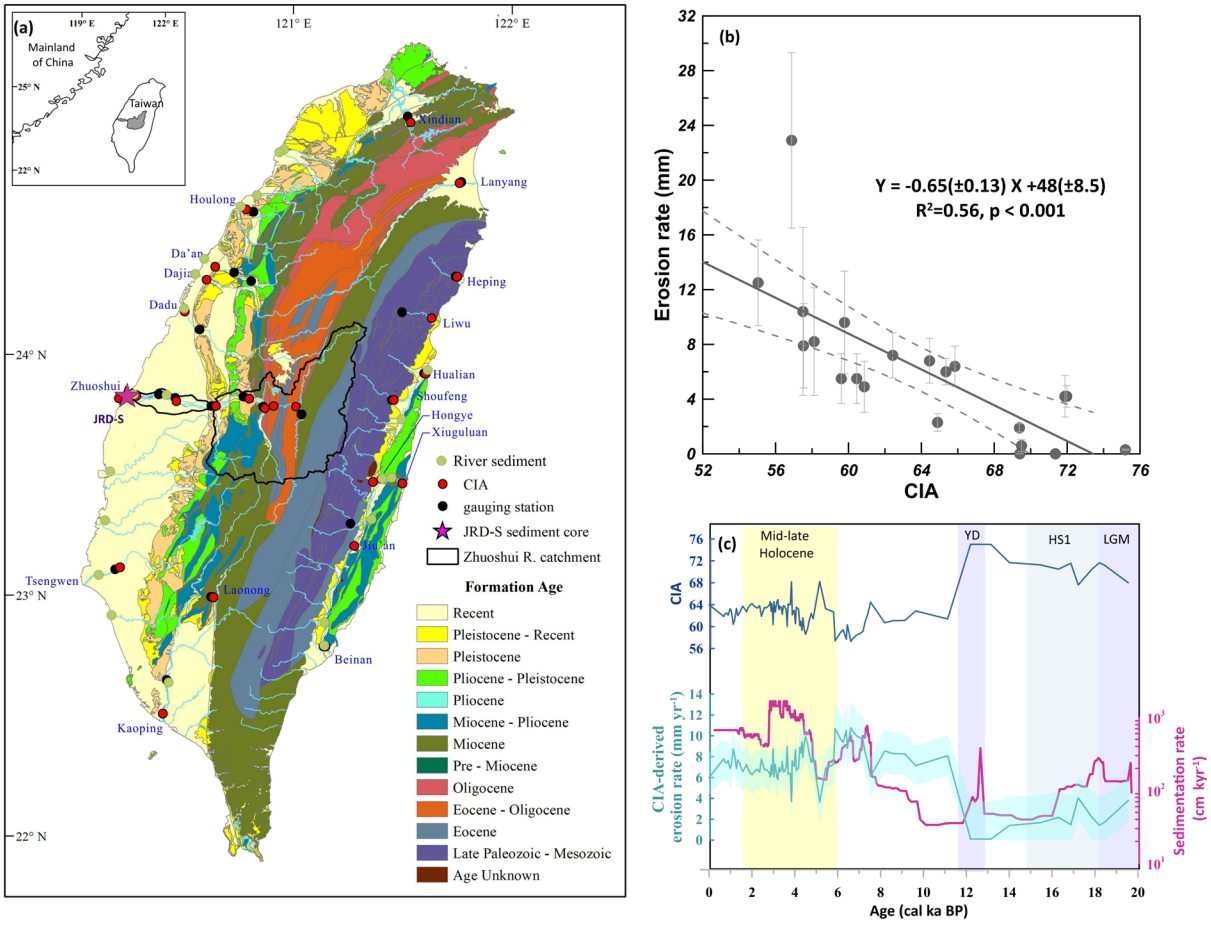


Figure 1 The geology map of Taiwan (Ho, 1986). (a) The purple star indicate the location of core JRD-S retrieved fromthe Zhuoshui River mouth; the green circles are the sites of river sediments (Lin et al., 2020), the black circles are the sites of chemimal index of alteration (CIA) data for river sediment (Garzanti and Resentini, 2016; Bi et al., 2015), the black circles are the gauging stations approaching the CIA data (Dadson et al., 2003).(b) The relationship between CIA and decadal erosion rate. CIA data from Garzanti and Resentini (2016) and Bi et al. (2015), and erosion rate data are from Dadson et al. (2003). (c) the temporal variation of CIA (blue curve, data from Zhao et al. (2017)), CIA-derived erosion rate (ice blue curve)(based on correlationship in b, shade is the 95% confidence interval), and sedimentation rate of JRD-S (purple curve).

The sediment core JRD-S, 104 m long, was taken from the south bank at the mouth of the Zhuoshui River delta (Latitude: 23.849 N, Longitude: 120.241 E; 4 m above sea level) (Figure 1). The details of sediment splitting, photographs, and description can be found in Yang et al. (2017). A high-resolution age model was established by ~40 radiocarbon measurements on tree branches, peat, and shell debris picked from different sediment depths (for details see Yang et al., 2017). The bayesian age–depth model for the JRD-S core was established using the BACON software package (Blaauw and Christen, 2011) based on radiocarbon data originally presented in Yang et al. (2017). Positioned at the mouth of the Zhuoshui River, an area known for its high physical erosion, we

anticipated that this core may hold a record of carbon source-sink dynamics. In light of this, we collected a total of 200 subsamples from the uppermost 60 m of the sediment core, at intervals of approximately 10-30 cm, for the purpose of conducting comprehensive geochemical analysis.

To assess how the effects of physical erosion and temperature influence TOC and radiocarbon (^{14}C) activity within Taiwan's contemporary landscape, we combine a number of published datasets. These included observations of TOC variations with altitude across 60 Taiwanese soil pedons (from Tsai et al., 2010; Tsui et al., 2013), vertical profiles of soil TOC and ^{14}C (Hemingway et al., 2018), ^{14}C compositions of river sediments (Lin et al., 2020), and erosion rate data for the watersheds (Dadson et al., 2003).

2.2 Geochemical analyses

2.2.1 Total organic carbon measurement.

For each sample, approximately 0.5 g of freeze-dried sediments were pre-treated with 2 N HCl to remove the calcium carbonate to obtain the total organic carbon content (TOC). The TOC was measured using an elemental analyzer (Flash 2000; Thermo Fisher Scientific) at a combustion temperature of 1020°C for a few seconds, at the National Taiwan Ocean University. Repeated analyses of a certified soil standard (certificate number 133317; Thermo Fisher Scientific) yielded a precision of 3% for TOC.

2.2.2 Radiocarbon measurements

Here, 14 samples were selected for radiocarbon measurements of the TOC. The radiocarbon composition measurements were conducted at the Beta Analytic Radiocarbon Dating Laboratory. The ^{14}C values have been corrected for $\delta^{13}C$ fractionation and are expressed as the fraction of modern carbon (Fm), relative to 95% of the ^{14}C activity of the NIST SRM-4990C (oxalic acid) standard. The measured Fm values and their associated uncertainties are detailed in Table 1.

The ^{14}C age of downcore TOC reflects a combination of the natural decay since the time of deposition and the ratio of the inputs of OC_{bio} and OC_{petro}, the latter being ^{14}C-depleted. The $F^{14}C$ difference between TOC and the sediment deposition can eliminate the effect of natural decay and indicates the ^{14}C of TOC at deposition time, which can reflect the mixture of contemporary and aged OC_{bio} with OC_{petro}. The fractional contribution of biospheric carbon (F_{bio}) was estimated using a binary mixing model (Equation 3). This model assumes that the OC_{bio} pool has a ^{14}C activity equivalent to the atmospheric ^{14}C activity ($F^{14}C_{atm.}$) at the time of deposition, while the OC_{petro} pool contains no radiocarbon. The estimated F_{bio} values and their propagated uncertainties are presented in Table 1. However, considering that the residence time of soil OC_{bio} in Taiwan ranges from 161 to 818 years (Hemingway et al., 2018; Lin et al., 2020), and the observed negative correlation between soil organic carbon residence time and both temperature and precipitation in worldwide soil ecosystems (Eglinton and Galy, 2021), it is implied that longer residence times occur during colder and dryer climates. Consequently, the assumption that the OC_{bio} pool mirrors the ^{14}C activity of the atmosphere at deposition could lead to an underestimation of F_{bio} and subsequently OC_{bio}, especially during such climatic periods. However, this underestimation appears to be less severe in Taiwan. For example, during cold and dry periods such as the YD and LGM, the F_{bio} of TOC at deposition could be as high as 0.93-0.99, which reflects that $F^{14}C_{TOC}$ can

achieve 93-99% of $F^{14}C_{atm.}$according to Equation (3).. Even if the TOC at these points consists entirely of OC_{bio} without any OC_{petro}, the underestimation would not exceed 8%. Future studies employing compound-specific ^{14}C analysis, such as ^{14}C-lignin or ^{14}C-plant wax, could further reduce uncertainties.

The $F^{14}C_{atm.}$ at the time of sediment deposition was obtained from the atmospheric $\Delta^{14}C$ reconstruction of IntCal 13, then the fractional contribution of biospheric carbon to TOC (F_{bio}) was estimated by the following equations:

$$TOC\% = OC_{bio}\% + OC_{Petro}\% \quad (1)$$

$$F^{14}C_{TOC} \times TOC\% = F^{14}C_{atm.} \times OC_{bio}\% + F^{14}C_{OC_{Petro}} \times OC_{Petro}\% \quad (2)$$

Since the OC_{petro} has no radiocarbon activity, $F^{14}C_{OCpetro} = 0$, the equation (2) can be rearranged as:

$$\frac{OC_{bio}}{TOC} = F_{bio} = \frac{F^{14}C_{TOC}}{F^{14}C_{atm.}} \quad (3)$$

The $F^{14}C_{TOC}$ denote the ^{14}C activity of TOC at sediment deposition time (Table 1). Accordingly, OC_{bio} is obtained by multiplying F_{bio} and TOC%, while OC_{petro} is gained by subtracting OC_{bio} from TOC.

Table 1 Radiocarbon data of TOC for sediment core JRD-S

Sample depth (cm below surface)	Deposition age (cal ky BP)*	$F^{14}C_{Atm.} \pm 1\sigma$[#]	$\Delta^{14}C_{TOC} \pm 1\sigma$ (‰)	$F^{14}C_{TOC} \pm \sigma$	F_{bio} at deposition	Age of TOC at deposition (yr)
1065-1066	1.61	0.8092 ± 0.0019	-901.24 ± 0.62	0.0996 ± 0.0006	0.1231 ± 0.0008	17714 ± 60
1502-1503	2.39	0.7407 ± 0.0034	-857.6 ± 0.89	0.1436 ± 0.0009	0.1939 ± 0.0015	13694 ± 61
1739-1740	2.85	0.7104 ± 0.0019	-890.36 ± 0.96	0.1106 ± 0.001	0.1557 ± 0.0015	14505 ± 79
2611-2612	3.47	0.6668 ± 0.0016	-933.28 ± 0.67	0.0673 ± 0.0007	0.1009 ± 0.0011	17872 ± 96
3266-3267	3.98	0.6369 ± 0.0017	-948.05 ± 0.52	0.0524 ± 0.0005	0.0823 ± 0.0008	19518 ± 91
4156-4157	5.87	0.5324 ± 0.0015	-917.35 ± 0.93	0.0833 ± 0.0009	0.1565 ± 0.0017	14374 ± 99
4580-4581	7.09	0.4637 ± 0.0014	-806.58 ± 0.97	0.195 ± 0.001	0.4205 ± 0.0025	6396 ± 59
5025-5026	9.19	0.3562 ± 0.0019	-887.73 ± 0.7	0.1132 ± 0.0007	0.3178 ± 0.0026	9359 ± 71
5162-5163	12.53	0.2747 ± 0.0011	-747.53 ± 0.95	0.2546 ± 0.001	0.9268 ± 0.0052	551 ± 64
5367-5368	16.37	0.1836 ± 0.0015	-935 ± 0.73	0.0655 ± 0.0007	0.3567 ± 0.0048	7150 ± 247
5536-5537	17.83	0.1595 ± 0.0021	-907.2 ± 0.68	0.0936 ± 0.0007	0.587 ± 0.0088	4361 ± 98
5575-5577	18.03	0.1606 ± 0.0037	-918.17 ± 0.76	0.0826 ± 0.0006	0.5142 ± 0.0125	5219 ± 102
5668-5669	18.38	0.1493 ± 0.0015	-853.1 ± 0.83	0.1481 ± 0.0009	0.9919 ± 0.0116	580 ± 97
5854-5855	19.71	0.1296 ± 0.0017	-943.67 ± 0.57	0.0568 ± 0.0006	0.4381 ± 0.0073	5881 ± 123

*Data from Yang et al. (2017).

[#] Data obtained from IntCal 13.

2.2.3 Net OC budget between the OC_{petro} oxidation and OC_{bio} yield

Under the influence of heavy rainfall-induced erosion, biospheric carbon from vegetation and soil enters rivers where it could be delivered to marine sediments, forming a carbon sink. At the same time, rock organic carbon exposed by deep erosion may be oxidized to a carbon source. We define the difference in yield per unit catchment area between these two processes as NET_{OC} (Equation 4), indicating the evolution of the source-sink pattern of mountain river carbon erosion. Although biospheric carbon export from mountain rivers can be efficiently buried in the deep sea under high turbidity and steep terrain (Kao et al., 2014; Zheng et al., 2017), its ultimate fate after exiting the river system is beyond the scope of this study and warrants further investigation. Therefore, we restrict our discussion of NET_{OC} to the relative changes in biogenic carbon export and fossil carbon oxidation within the catchment.

The temporal variation of the net OC budget (NET_{OC}) between the OC_{petro} oxidation ($J_{OCpetro-ox}$) and OC_{bio} yield (J_{OCbio}) can be expressed as:

$$NET_{OC} = J_{OCpetro-ox} - J_{OCbio} \quad (4)$$

The OC_{petro} component can be considered as either oxidized ($J_{OCpetro-ox}$), or exported in the river solid load ($J_{OCpetro}$). We collate data from 11 rivers in Taiwan which include measurements of solid $J_{OCpetro}$ that increases linearly with the suspended sediments yield (SSY, Hilton et al., 2011). Meanwhile, OC_{petro} oxidation rates, estimated using the trace element rhenium as a proxy, suggest that the $J_{OCpetro-ox}$ rate is also correlated with SSY (Hilton et al., 2014). For 10 catchments in Taiwan where $J_{OCpetro-ox}$ and $J_{OCpetro}$ were synchronously measured, we found a statistically significant linear correlation between $J_{OCpetro-ox}$ and $J_{OCpetro}$ (Figure 2a). This correlation combined with CIA-derived erosion rate (Figure 1b) enables us to infer the historical changes of $J_{OCpetro-ox}$ and subsequently, the NET_{OC}.

This relationship appears robust for Taiwan as it is based on the observations across 10 different catchments, despite large differences in suspended loading (ranging from 2000 to 30,000 t km^{-2} yr^{-1}), catchment area (150 to 1500 km^2), bedrock type and erodibility, and vegetation cover. Given that physical erosion primary controls both OC_{petro} export and oxidation (Hilton et al., 2014; Hilton, 2016), changes within the same river during millennial timescales are unlikely to exceed this observed range. However, we also acknowledge that the empirical relationship used in Figure 2 is based on decadal-scale modern observations, and its applicability on centennial or millennial timescales requires further investigation. Furthermore, the recently proposed $^{10}Be/^{9}Be$ ratio presents a promising tool for reconstructing millennial-scale erosion rates (Deng et al., 2019,2020), which could complement our current approach.

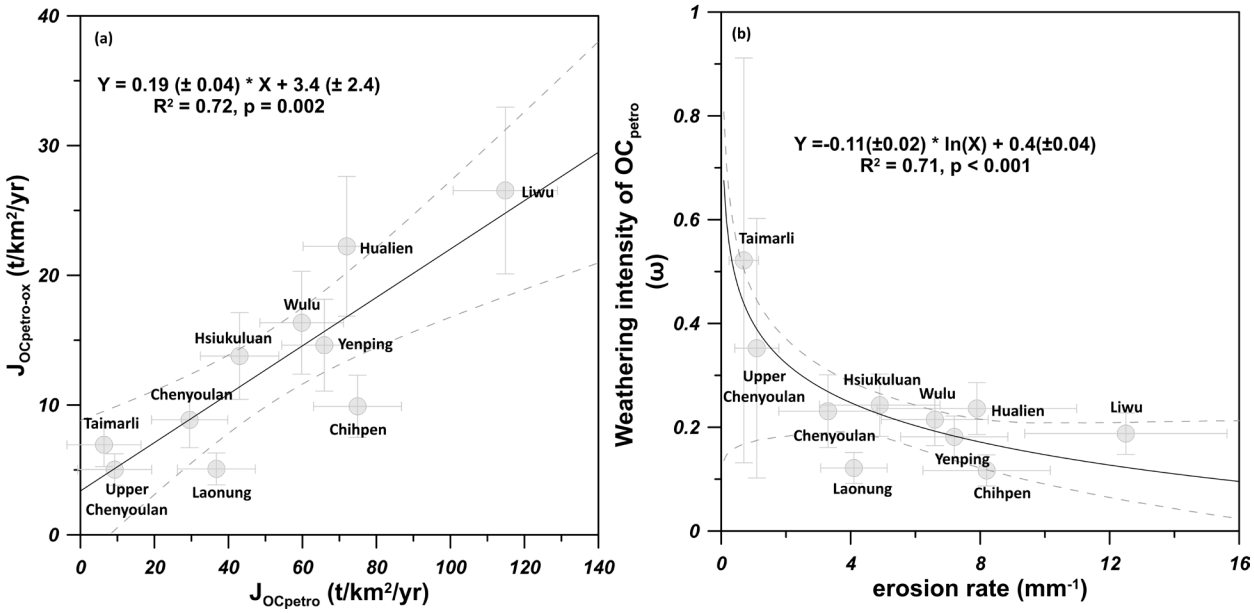


Figure 2 Physical erosion control the OC_{petro} oxidation and export. (a) An empirical relationship between the flux of petrogenic OC oxidation ($J_{OCpetro\text{-}ox}$) and petrogenic OC yield ($J_{OCpetro}$). (b) the relation between erosion rate and weathering intensity of OC_{petro}. The OC_{petro} oxidation data of different rivers is from Hilton et al. (2014), while the OC_{petro} yield data of the same rivers was derived from Hilton et al. (2011).The erosion rate is obtained from Dadson et al. (2003). The solid lines in the figures indicate the regression, while the dashed lines representing the 95% confidence interval of the regression.

To evaluate the oxidation of OC_{petro}, we calculate the ratio of OC_{petro} oxidation flux to total OC_{petro} initially available, representing a metric of weathering intensity of OC_{petro}, denoted as ω:

The ω can be written as:

$$\omega = \frac{J_{OCpetro-ox}}{J_{OCpetro-ox} + J_{OCpetro}} (5)$$

So:

$$J_{OCpetro-ox} = \frac{\omega}{(1-\omega)} \times J_{OCpetro} \ (6)$$

The $J_{OCpetro}$ and J_{OCbio} can be calculated using:

$$J_{OCpetro} = OC_{petro}\% \times SSY \ (7)$$

$$J_{OCbio} = OC_{bio}\% \times SSY \quad (8)$$

In a carbon-neutral state where $NET_{OC} = 0$, Equation (4) can be rearranged to:

$$J_{OCbio} = \frac{\omega}{(1-\omega)} \times J_{OCpetro} \ (9)$$

Then, by substituting the equation (1), (7), and (8) into Equation (9), we can further rearrange it as:

$$SSY \times OC_{bio}\% = \frac{\omega}{(1-\omega)} \times SSY \times OC_{petro}\ \% \quad (10)$$

$$OC_{bio}\% = \frac{\omega}{(1-\omega)} \times (TOC\% - OC_{bio}\%) \quad (11)$$

This now allows us to consider a OC_{bio}/TOC ratio for which the net CO_2 balance will be 0 for a given intensity of OC_{petro} oxidation (ω). We define this as a critical value of F_{bio}, $F_{bio\text{-}critical}$:

$$\frac{OC_{bio}\%}{TOC\%} = F_{bio-critical} = \omega \quad (12)$$

These equations reveal that if the ω value is 0.9 (intense weathering of OC_{petro}), the F_{bio} value of the sediment being exported would need to be >0.9 to result in a sink of CO_2 by the organic carbon cycle. Contrary, if the ω value is 0.1 (less intense weathering of OC_{petro}, the F_{bio} value would have to be >0.1 for the erosional system to be a CO_2 sink.

We have direct measurement of F_{bio} in the core using bulk radiocarbon and the chronology (Table 1), and we can estimate ω using empirical equation in Figure 2b. This allows us to explore the offsets between ω and F_{bio} through time, and assess the net balance between OC_{petro} oxidation and OC_{bio} export. If $F_{bio} > \omega$ at a point in the record, the system is acting as a CO_2 sink, whereas if $F_{bio} < \omega$, there is a net CO_2 source. It is important to note that this metric reflects a net balance, and does not reconstruct the magnitude of fluxes. For instance, decling F_{bio} values could be occurring in a backdrop of increasing OC_{bio} fluxes, but the shift results from OC_{petro} fluxes that are increasing more rapidly. Similarly, the decline in ω signifies a decrease in oxidation weathering intensity but does not necessarily imply a decrease in oxidation flux. Modern observations also show that ω decreases with increasing physical erosion (Figure 2b), while the oxidation flux of OC_{petro} is positively correlated with physical erosion (Hilton et al., 2014).

3 Results and Disussion

3.1 Assessing Past Variability in Erosion using Sediment Geochemistry

The age model suggests a high sedimentation rate during the Holocene with a sediment thickness of ~43m deposited within 11.6 kyr (~0.37cm yr^{-1}), and a ~5x lower deposition rate during the deglacial period(~0.07cm yr^{-1}) (Figure 1c).

However, a sedimentary unconformity is observed in the early Holocene of the JRD-S core, which may be linked to an intensified hydrodynamic setting that hindered sediment deposition at this location (Yang et al., 2017). This contrasts with sedimentary records from lakes in Taiwan and offshore areas during the early Holocene, which indicate high deposition rates under warm and humid climatic conditions (Yang et al., 2011). Thus, assessing changes in physical erosion

based solely on variations in deposition rates during the deglacial and Holocene periods may introduce uncertainties.

Previous research has indicated that under conditions of heightened physical erosion, minerals may not undergo sufficient chemical weathering, resulting in a decline in the Chemical Index of Alteration (CIA) (Zhao et al., 2017; McLennan, 1993). To address this, we compiled CIA data from river sands at 22 major river mouths in Taiwan (Garzanti and Resentini, 2016), and paired it with decadal physical erosion rate data from gauging stations closest to the CIA sampling points following the dataset provided by Dadson et al. (2003) (see Figure 1a). Our analysis revealed a negative correlation between CIA values and erosion rates (Figure 1b).

Within the JRD-S core, during the Holocene period, the mean CIA value averaged 62 ± 2, whereas during the deglacial period, it was 71 ± 3 (Zhao et al., 2017). This shift in CIA values between the deglacial and Holocene periods suggests that the erosion rate during the deglacial period was approximately 4 times lower (ranging from 0 to 4 mm) compared to the Holocene period (ranging from 4 to 10 mm), in accordance with the established correlation between CIA values and erosion rates (Figure 1b).

Furthermore, the CIA-derived erosion rate indicates higher values during the early Holocene period (from 11.6 to 8 cal ka BP, Figure 1c). This observation aligns with previous studies that have documented an increase in the frequency of tropical cyclones (typhoons) during the early Holocene, substantiated by the presence of ancient landslide records (Hsieh et al., 2012, 2014), elevated sea spray signals recorded in Taiwan's lake sediments (Ding et al., 2016b), and a high frequency of turbidite records offshore Taiwan (Yu et al., 2017). Consequently, it is reasonable to posit that the CIA-derived erosion rate may provide a more representative indicator of changes in physical erosion since the last glacial period.

3.2 The Influence of Precipitation and Temperature on Radiocarbon Composition of Soil and River Suspended OC in modern Taiwan

Soil profiles in Taiwan exhibit a logarithmic decrease in TOC and F_{bio} of TOC with depth (Figure 3a, b). The decrease in F_{bio} with depth in the soil profile is associated with the combined effects of biomass-derived OC_{bio} incorporation, aging of OC_{bio}, and degradation of organic carbon during soil formation processes (Hemingway et al., 2018). Consequently, we hypothesize that intense erosion, induced by heavy rainfall, might unearth more particles with lower TOC% and F_{bio}, hence diluting these values in suspended and river sediment loads. This process would be reversed during periods of lower physical erosion. The F_{bio} of TOC in river sediments near major river mouths in Taiwan (Lin et al., 2020) displays a negative trend with decadal suspended sediment yield (SSY, from Dadson et al., 2003) (Figure 3c). Furthermore, contemporary observations document decreasing TOC% values with increasing physical erosion (Figure 3d)

(Milliman et al., 2017; Hilton et al., 2012; Kao and Milliman, 2008), substantiating the aforementioned hypothesis.

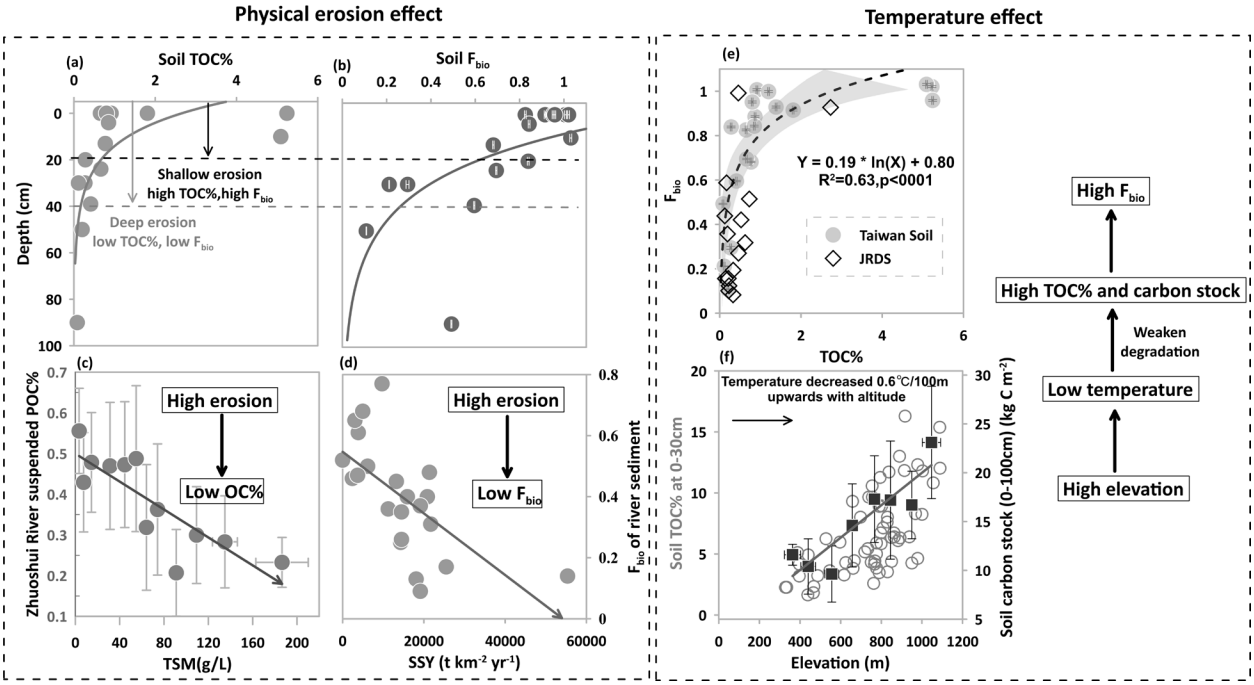


Figure 3. Impact of Physical Erosion and Temperature on Radiocarbon Composition of Soil and Suspended Organic Carbon in Modern Taiwan. (a) Vertical depth profile of total organic carbon (TOC) in Taiwan soils (Hemingway et al., 2018); (b) Soil profiles of F_{bio} (fraction modern) in Taiwan (Hemingway et al., 2018). Solid lines in (a) and (b) represent logarithmic regressions of TOC and F_{bio} with depth, respectively, while dashed lines illustrate the characteristics of TOC and F_{bio} at different erosion depths. (c) Particulate organic carbon (POC) content versus total suspended material in the Zhuoshui River (Milliman et al., 2017). The arrow indicates a decrease in POC% with increasing erosion. (d) F_{bio} of river sediments around Taiwan (Lin et al., 2020) versus decadal suspended sediment yield (Dadson et al., 2003). The arrow shows a decrease in F_{bio} with increasing erosion. (e) TOC versus F_{bio} (dots represent Taiwan soil data from (a) and (b), diamonds represent data from JRD-S). The dashed line indicates the natural logarithmic regression of TOC and F_{bio}, with the gray shade representing the 95% confidence interval of the regression. (f) Elevational variation of soil carbon stock (0-100cm) and shallow soil TOC% (data from Tsui et al., 2013). Solid lines in (f) indicate the linear regression between soil carbon stock (0-100cm) and elevation.

The positive correlation between F_{bio} and TOC% is evident in both Taiwan soils and the sediment core JRD-S (Figure 3e). This correlation suggests that a higher TOC% comprises a greater proportion of OC_{bio} as opposed to OC_{petro}.

Moreover, previous studies have revealed a positive correlation between soil organic carbon inventory (0-100 cm) and elevation, as well as between shallow TOC% (0-30 cm) and elevation, across Taiwan based on data from 60 soil pedons (Tsai et al., 2010; Tsui et al., 2013) (Figure 3f). The soil organic carbon inventory represents the net effect of accumulation (e.g., litterfall input, root input) and degradation processes. Notably, litterfall, which plays a crucial role in recycling dead organic matter and nutrients back into the soil organic carbon pool, exhibits a negative correlation with elevation (Wang et al., 2016). This trend is attributed to the elevation effect on air

temperature and vegetation types; higher elevations typically support biomes with lower biomass density, resulting in reduced litterfall and live carbon storage (Brown and Lugo, 1982; Chiu et al., 2014). Consequently, our results suggest that temperature induced degradation, rather than the accumulation process, is the dominant factor influencing the positive relationship between soil carbon storage and elevation (Tsui et al., 2013). This observation aligns with broader research indicating that temperature plays a crucial role in controlling soil carbon stocks in mid to high latitude regions (Melillo et al., 2002; Lloyd and Taylor, 1994). In Taiwan, temperature exhibits a decrease of approximately 0.6 - 0.7 ℃ per 100 meters of increased altitude, creating cooler conditions that inhibit soil respiration rates (Huang et al., 2017). Consequently, these conditions favor the preservation of TOC%.

In contrast, lower elevation sites experience higher temperatures, which intensify organic carbon degradation, resulting in lower observed TOC% and F_{bio}. The positive relationship between elevation, TOC%, and F_{bio} collectively suggests that the degradation of OC_{bio} is more sensitive to temperature fluctuations than that of OC_{petro}.

Measurements of OC_{petro} oxidation at rock outcrops in New Zealand and France suggest a temperature control on oxidation rate (Roylands et al., 2022), confirming labatorary incubations (Chang and Berner, 1999; Tune et al., 2023). However, OC_{petro}, primarily composed of kerogen from geological sources, displays minimal biological activity after being exposed to high temperatures and pressures during mountain-building processes (Blair and Aller, 2012). In contrast, OC_{bio}, originating from terrestrial ecosystem productivity, is more labile in nature than OC_{petro} (Blair and Aller, 2012). This difference in resistance might potentially explain the higher temperature sensitivity of OC_{bio} degradation compared to OC_{petro} oxidation.

In summary, both climatic warming and increased physical erosion in a catchment could lead to a reduction in suspended particulate organic carbon F_{bio} through i) an increased erosion depth; ii) preferential degradation of soil OC_{bio} over OC_{petro} as climate warms.

Temperature and rainfall have varied over the past 20 kyr in the Taiwan region (Liew et al., 1998, 2006; Li et al., 2013). This provides an opportunity to examine the primary driver for particulate organic carbon and its F_{bio} in the past. It is also worth mentioning that previous studies have shown that in high-erosion and rapid-deposition systems like Taiwan, the preservation efficiency of organic carbon in coastal sediments is remarkably high (Kao et al., 2014). There is almost no post-depositional diagenetic influence (Kao et al., 2014). Hence, the TOC and F_{bio} of

estuarine sediments reflect the influence of climate change on the catchment's organic carbon and radiocarbon composition.

3.3 Climate regulation of TOC and F_{bio} since the Last Glacial Maximum

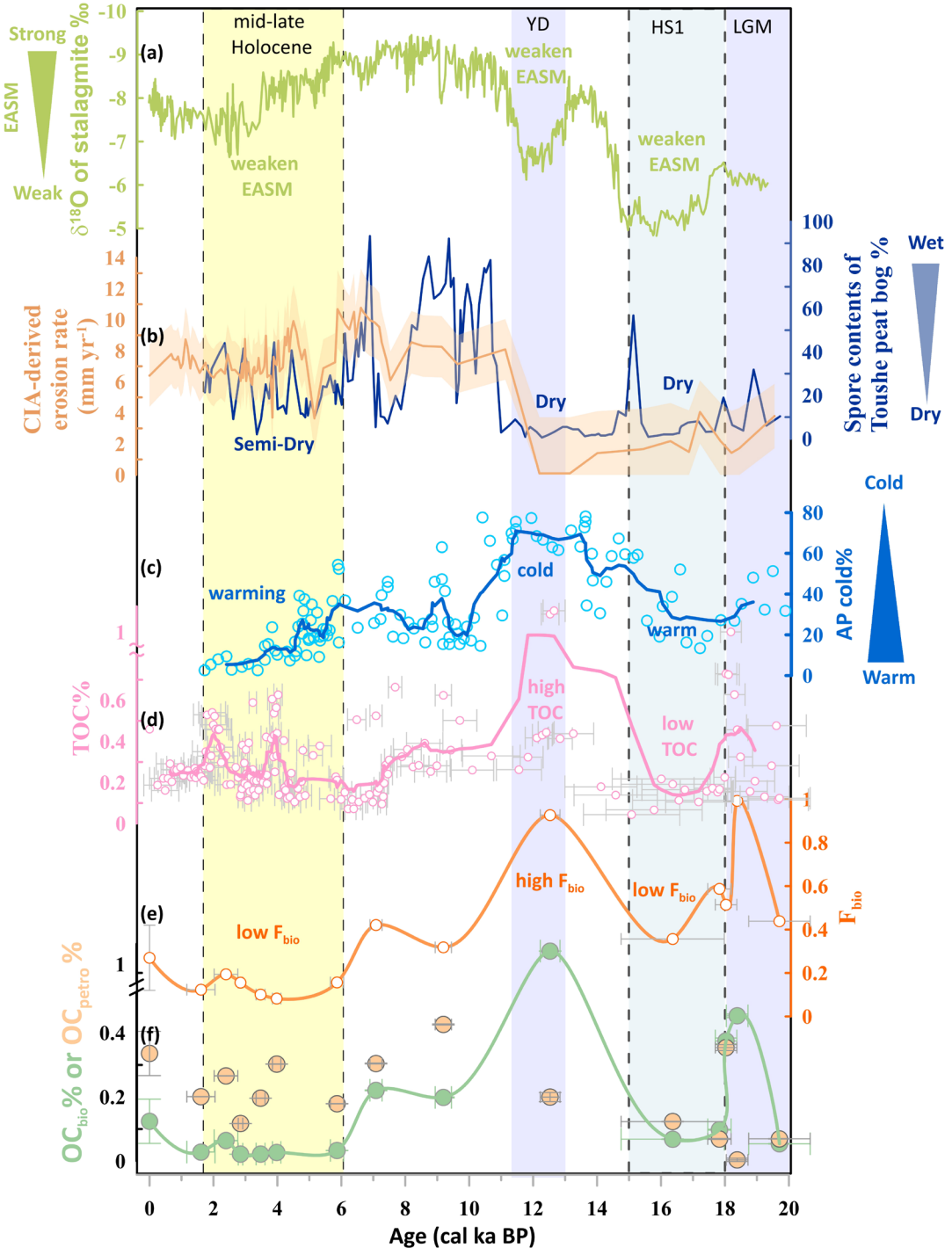


Figure 4 Temporal variations of (a) stalagmite oxygen isotope from Hulu Cave and Dongge Cave (Wang et al., 2001; Dykoski et al., 2005), (b) spore contents in Toushe peat bog in central Taiwan (blue curve)

(Liew et al., 2006); CIA-derived erosion rate (yellow curve, shading indicates propagated uncertainties), (c) proportion of arboreal pollen families favoring colder conditions (AP cold%) from the Toushe peat bog (Li et al., 2013),the blue curve indicates the 9 points running average (d) total organic carbon (TOC%) the pink curve indicates the 9 points running average, (e) fraction of biospheric OC (F_{bio}), and (f) the biospheric organic carbon content (OC_{bio}%).

The East Asian Summer Monsoon, as denoted by the $\delta^{18}O$ of stalagmites from the Dongge and Hulu caves, has generally strengthened from the Last Glacial Maximum (LGM) to the Holocene (Wang et al., 2001; Dykoski et al., 2005) (Figure 4a). However, there were intermittent periods of weakened monsoon activity, most notably during the Heinrich Stadial 1 (HS1) and Younger Dryas event (YD). The monsoon reached its peak in the early Holocene (11.6-8 cal ka BP), experienced a weakening phase during the mid-to-late Holocene (6-2 cal ka BP), and has been strengthening again since the late Holocene (since 2 cal ka BP).

Correspondingly, monsoon-driven rainfall intensity, indicated by spore content from the Toushe peat bog in central Taiwan (Liew et al., 2006), suggests that Holocene conditions were generally more humid than during the deglaciation period (Figure 4b). Consistent with the pattern of rainfall intensity, the physical erosion rate during the deglacial period remained relatively low, with values typically ranging from 0 to 4 mm yr^{-1}. The erosion rate was exceptionally low during the YD and HS1. In contrast, during the Holocene period, which coincided with an intensified EASM and increased precipitation, physical erosion rates significantly increased, reaching values between 4 and 10 mm yr^{-1}.

Simultaneously, temperature variations, as indicated by the proportion of arboreal pollen families favoring colder conditions (AP cold%) derived from the Toushe peat bog in central Taiwan (Figure 4c), suggest that temperatures were higher during the Holocene compared to the deglaciation period (Li et al., 2013).

The trends of TOC%, F_{bio}, and OC_{bio}% over the past 20 kyr exhibit similar patterns, with generally higher values during the deglacial periods than during the Holocene (Figure 4d, 4e, 4f). These higher values during cold and dry periods, such as the LGM and the YD, can be attributed to shallow erosion and the enhanced preservation of TOC and OC_{bio} under cold conditions. However, during the HS1 period, pollen records from Taiwan suggest that the climate was extremely dry but not as cold as during the YD period (Figure 3b, Li et al., 2013). This relatively warm condition favored the preferential degradation of OC_{bio}, leading to lower values in TOC%, F_{bio}, and OC_{bio}% compared to the YD period.

Since the onset of Holocene (11.6 cal ka BP), increased precipitation and warming have resulted in lower values for TOC%, F_{bio}, and OC_{bio}% (Figure 4d, 4e, 4f). This trend can be attributed to a combination of factors, including dilution due to deeper erosion and preferential degradation of OC_{bio} under warm condition. During the early to mid-Holocene (11.6 to 6 cal ka BP), as the EASM gradually intensified, both rainfall and erosion gradually increased to their maximum levels. TOC, F_{bio}, and OC_{bio}% consequently declined during this period. Notably, given the relatively constant temperature during this time (Figure 4c), this trend can be explained by the

deepening of physical erosion, resulting in lower TOC% and OC_{bio}% content in the deeper soil layers.

In contrast, during the mid-to-late Holocene, the EASM weakened (Figure 4a), leading to a subsequent decrease in rainfall intensity and physical erosion. Simultaneously, the climate continued to warm (Figure 4c) when compared to the early to mid-Holocene period. During this period, TOC% increased and reached relatively high levels (ranging from 0.2% to 0.6%). However, F_{bio} and OC_{bio}% exhibited their lowest values during this time, implying that the warming climate favored the preferential degradation of OC_{bio}% over OC_{petro}%, nearly depleting OC_{bio}%.

In contrast to the variations observed in TOC% and OC_{bio}%, OC_{petro}% content consistently showed lower values during the deglacial period compared to the Holocene (as depicted in Figure 4f), with extremely low values (<0.1%) during the dry periods (LGM and HS1), indicating shallow erosion and intense oxidation in catchment.

In summary, the elevated values of TOC%, F_{bio}, and OC_{bio}% during deglacial cold and dry periods suggest weaker erosion and better organic matter preservation under such climatic

conditions. Conversely, during warmer and wetter periods such as the Holocene, increased rainfall led to deeper erosion and more pronounced organic matter oxidation.

3.4 Carbon Balance Between OC_{petro} Oxidation and OC_{bio} Export

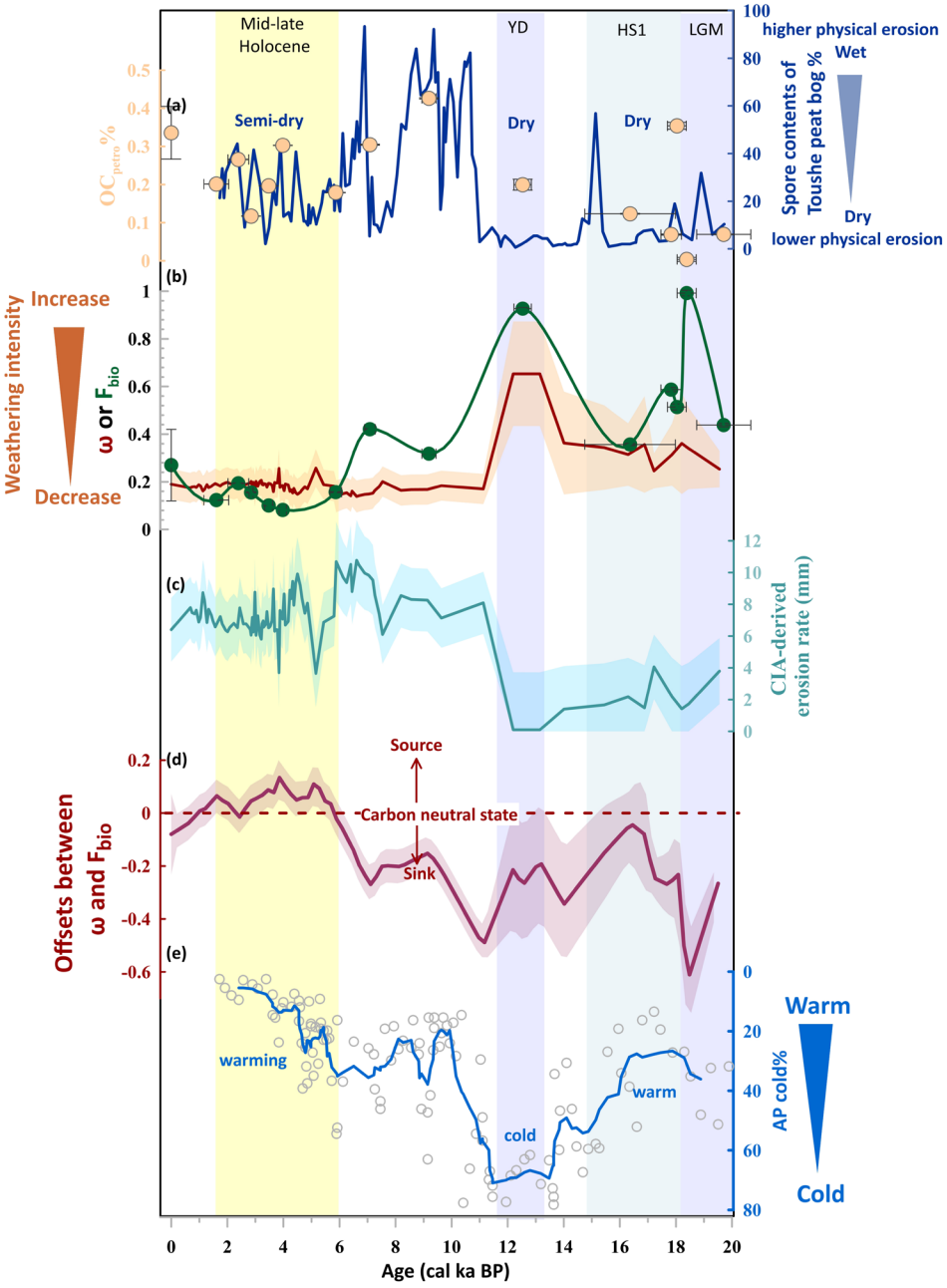


Figure 5. The temporal variations of (a) OC_{petro} (orange circles) and spore contents in Toushe peat bog in central Taiwan (blue curve) (Liew et al., 2006); (b) the weathering intensity of OC_{petro} (ω)(orange, with shading representing uncertainties), F_{bio} (green, the error bars smaller than symbols), (c) CIA-derived erosion rate (shading represents the 95% confidence interval), (d) offsets between ω and F_{bio} (shading

458 indicates propagated uncertainties); (e) proportion of arboreal pollen families favoring colder conditions
459 (AP cold%) from the Toushe peat bog (Li et al., 2013).

460 As previously stated, although temperature modulates particulate organic carbon content and
461 composition, physical erosion determines the export flux of OC_{bio} and oxidation of OC_{petro}, thereby
462 shaping the source-sink pattern of fluvial carbon erosion.

463 As illustrated in Figure 5a, the variations in OC_{petro} exhibit synchronicity with rainfall
464 intensity, while the weathering intensity of OC_{petro}, ω, demonstrates an inverse relationship with
465 rainfall intensity. This observation suggests that the intensification of physical erosion diminishes
466 the efficiency of OC_{petro} oxidation. Based on this core record, it appears that while weathering
467 intensity of OC_{petro} declined by ~50% from the deglacial period into the Holocene (from $\omega \sim 0.38 \pm 0.13$ to $\omega \sim 0.18 \pm 0.02$), the overall sediment accumutation rate increased by ~5 times (erosion
469 rate increased by ~4 times, Figure 1c), suggesting an overall increase in weathering fluxes. The
470 greater fluxes of OC_{petro} oxidation are consistent with an overall supply-limited process, where
471 increases in physical erosion can be accompanied by increased weathering rates (Hilton et al.,
472 2014). In addition, they are consistent with recent work showing warmer temperatures can increase
473 OC_{petro} oxidation rates (Soulet et al., 2021; Roylands et al., 2022).

474 Simultaneously, F_{bio} exhibits a similar variation pattern to ω (Figure 5b), with values
475 declining by 69% from the deglacial period to the Holocene (from $F_{bio} \sim 0.64 \pm 0.24$ to $F_{bio} \sim 0.20 \pm 0.11$). Following the change of F_{bio}, we see a dramatic fall in the concentration of OC_{bio} in
477 sediments at the core site. A ~7x decline in OC_{bio} from 0.6 ± 0.8% to 0.08 ± 0.07% from the
478 deglacial to the Holocene (Figure 3f) happened while the physical erosion rates increased ~4 - 5
479 times. This suggests the J_{OCbio} did slightly decrease over this time period. As previously discussed,
480 this could reflect lower OC_{bio} stocks in soils of the landscape as the temperature warmed. It could
481 also reflect an increase in erosion depth, meaning increased sediment export did not accompany
482 any increased surface soil and vegetation erosion. This is seen in global river yield data, where the
483 highest sediment yields have proportionally less OC_{bio} export (Galy et al., 2015).

484 The temporal variations in the offsets between ω and F_{bio} qualitatively describe the evolution
485 of NET_{OC} (Figure 5d). We observe that during periods characterized by cold and dry conditions,
486 such as the YD and LGM, despite the large uncertainties, the net balance shows a CO_2 sink. This
487 CO_2 sink might be even higher than we show in the Figure 5d. As discussed above, the OC_{bio} (and
488 thus NET_{OC}) might be underestimated by up to 8% due to the longer residence time of OC_{bio} during
489 cold and dry periods. In contrast, during warm and dry periods, like the mid-late Holocene, the
490 balance shifts towards a CO_2 source. This pattern is regulated by both temperature and erosion
491 (Figure 5c, 5e). It is apparent that temperature plays a more pronounced role in this regulation. Our
492 findings illustrate that NET_{OC} follows a pattern closely aligned with temperature fluctuations,
493 transitioning from warm to cold from the HS1 to the YD, and then from cold to warm during the
494 early Holocene to the mid-Holocene periods. Notably, the conspicuous change in CIA-derived
495 physical erosion, predominantly occurs in a brief period after the YD. Throughout the Holocene,

we do not observe a significant upward trend in erosion, though it broadly mirrors the NET_{OC} trend from the deglacial to the Holocene period.

Overall, the increased physical erosion and climate warming during the deglaciation into the Holocene appears to have pushed Taiwan towards a net source of CO_2. This occurred through competing effects on OC_{bio} stocks, OC_{bio} erosion versus OC_{petro} oxidation.

4. Conclusion

Our study highlights the dynamic trade-off between biospheric and rock-derived carbon in the carbon cycle, during mountain erosion. In subtropical Taiwan, we synthesize modern field observations and sediment core analyses to provide novel insights into the carbon dynamics across significant climatic transitions, particularly the last deglaciation. We demonstrate that the riverine export of OC_{bio} and the oxidation of OC_{petro} are heavily influenced by physical erosion, which itself is modulated by climatic factors such as precipitation and temperature. Our findings suggest that the global carbon balance is sensitive to these environmental changes, with varying impacts on different carbon sources.

During the last deglaciation, the elevated TOC%, F_{bio}, and OC_{bio}% values during colder and drier periods suggest more efficient organic matter preservation under these climatic conditions. Conversely, the warmer and wetter Holocene period saw increased rainfall, leading to more pronounced organic matter oxidation and a shift toward carbon source in the carbon balance.

Our analysis of the OC_{petro} oxidation and OC_{bio} export net balance reveals that during the deglaciation into the Holocene, Taiwan likely shifted towards being a net source of CO_2. This shift was driven by the competing effects of OC_{bio} erosion and OC_{petro} oxidation, exacerbated by increased physical erosion and climatic warming.

In conclusion, this study underscores the critical role of environmental factors in shaping carbon dynamics in erosion-prone regions. It highlights the need for a deeper understanding of the interplay between biospheric and rock-derived carbon in the face of ongoing climatic changes. Our findings are particularly relevant for predicting how subtropical regions, like Taiwan, will respond to the continuous rise in atmospheric CO_2 and the associated climatic shifts, potentially transforming these areas into significant carbon sources in the global carbon cycle.

Acknowledgments, Samples, and Data

This research was supported by the Hainan Province Science and Technology Special Fund (ZDYF2022SHFZ112), National Natural Science Foundation of China (NSFC 42266002, 41806062, 41876076, 41721005, 42276061 and 91858209), National Postdoctoral Program for Innovative Talents of china (BX201700139), and China Postdoctoral Science Foundation (2018M642567). RGH was supported by the European Research Council (ERC Starting Grant, ROC-CO_2, #678779). Xufeng Zheng was supported by the Hainan Province Science and Technology Special Fund (ZDYF2022SHFZ091) The funding for drilling the JRD-S core was provided by the ROC Ministry of Science and Technology under the grant numbers: NSC 99-2611-M-110-005, NSC 100-2611-M-110-013 to JTL. All the original data can be found in supplementary dataset and also will be available from the data share website after the manuscript is accepted.

Declaration of generative AI and AI-assisted technologies in the writing process

During the preparation of this work the Li-Wei Zheng used ChatGPT to conduct grammar checks and enhance language fluency for improved readability. After using this tool/service, the Li-Wei Zheng reviewed and edited the content as needed and take(s) full responsibility for the content of the publication.

References

Blaauw, M., & Christen, J. A. (2011). Flexible Paleoclimate Age-Depth Models Using an Autoregressive Gamma Process. *Bayesian Analysis, 6*(3), 457-474.

Bi, L., Yang, S., Li, C., Guo, Y., Wang, Q., Liu, J. T., & Yin, P. (2015). Geochemistry of river-borne clays entering the E ast C hina S ea indicates two contrasting types of weathering and sediment transport processes. *Geochemistry, Geophysics, Geosystems, 16*(9), 3034-3052.

Blattmann, T. M., D. Letsch, and T. I. Eglinton (2018), On the geological and scientific legacy of petrogenic organic carbon, American Journal of Science, 318(8), 861-881.

Blair, N. E., and R. C. Aller (2012), The fate of terrestrial organic carbon in the marine environment, *Annual review of marine science*, *4*, 401-423, doi:10.1146/annurev-marine-120709-142717.

Bouchez, J., O. Beyssac, V. Galy, J. Gaillardet, C. France-Lanord, L. Maurice, and P. Moreira-Turcq (2010), Oxidation of petrogenic organic carbon in the Amazon floodplain as a source of atmospheric CO2, Geology, 38(3), 255-258, doi:10.1130/g30608.1.

Brown, S., and A. E. Lugo (1982), The storage and production of organic matter in tropical forests and their role in the global carbon cycle, *Biotropica*, 161-187.

Burdige, D. J. (2005), Burial of terrestrial organic matter in marine sediments: A re-assessment, *Global Biogeochemical Cycles*, *19*(4).

Chang, S., & Berner, R. A. (1999). Coal weathering and the geochemical carbon cycle. *Geochimica et Cosmochimica Acta, 63*(19), 3301-3310.

Dadson, S. J., N. Hovius, H. Chen, W. B. Dade, M.-L. Hsieh, S. D. Willett, J.-C. Hu, M.-J. Horng, M.-C. Chen, and C. P. Stark (2003), Links between erosion, runoff variability and seismicity in the Taiwan orogen, *Nature*, *426*(6967), 648-651.

Derry, L. A., & France-Lanord, C. (1996). Neogene growth of the sedimentary organic carbon reservoir. *Paleoceanography, 11*(3), 267-275.

Ding, X., D. Li, L. Zheng, H. Bao, H.-F. Chen, and S.-J. Kao (2016a), Sulfur Geochemistry of a Lacustrine Record from Taiwan Reveals Enhanced Marine Aerosol Input during the Early Holocene, Scientific reports, 6, doi:10.1038/srep38989.

Ding, X., L. Zheng, D. Li, T.-N. Yang, T.-Q. Lee, and S.-J. Kao (2016b), Lacustrine record of centennial-and millennial-scale rainfall variability of the East Asian summer monsoon during the last deglaciation: Multi-proxy evidence from Taiwan, Palaeogeography, Palaeoclimatology, Palaeoecology, 450, 38-49, doi:10.1016/j.palaeo.2016.02.048.

Ding, X., L. Zheng, X. Zheng, and S. Kao (2020), Holocene East Asian summer monsoon rainfall variability in Taiwan, *Frontiers in Earth Science*, *8*, 234.

Dykoski, C., Edwards, R., Cheng, H., Yuan, D., Cai, Y., Zhang, M., et al. (2005). A high-resolution, absolute-dated Holocene and deglacial Asian monsoon record from Dongge Cave, China. Earth and Planetary Science Letters, 233(1-2), 71-86.

Eglinton, T. I., V. V. Galy, J. D. Hemingway, X. Feng, H. Bao, T. M. Blattmann, A. F. Dickens, H. Gies, L. Giosan, and N. Haghipour (2021), Climate control on terrestrial biospheric carbon turnover, *Proceedings of the National Academy of Sciences*, *118*(8), e2011585118.

Galy, V., O. Beyssac, C. France-Lanord, and T. Eglinton (2008), Recycling of graphite during Himalayan erosion: A geological stabilization of carbon in the crust, Science, 322(5903), 943-945.

Galy, V., B. Peucker-Ehrenbrink, and T. Eglinton (2015), Global carbon export from the terrestrial biosphere controlled by erosion, Nature, 521(7551), 204-207, doi:10.1038/nature14400.

Garzanti, E., & Resentini, A. (2016). Provenance control on chemical indices of weathering (Taiwan river sands). *Sedimentary Geology, 336*, 81-95.

587 Goldsmith, S. T., A. E. Carey, W. B. Lyons, S.-J. Kao, T.-Y. Lee, and J. Chen (2008), Extreme storm events,
588 landscape denudation, and carbon sequestration: Typhoon Mindulle, Choshui River, Taiwan, *Geology*, *36*(6),
589 483-486.
590 Hedges, J. I., and R. G. Keil (1995), Sedimentary organic matter preservation: an assessment and speculative
591 synthesis, *Marine chemistry*, *49*(2-3), 81-115, doi:10.1016/0304-4203(95)00008-F.
592 Hein, C. J., M. Usman, T. I. Eglinton, N. Haghipour, and V. V. Galy (2020), Millennial-scale hydroclimate control
593 of tropical soil carbon storage, *Nature*, *581*(7806), 63-66, doi:10.1038/s41586-020-2233-9.
594 Hemingway, J. D., R. G. Hilton, N. Hovius, T. I. Eglinton, N. Haghipour, L. Wacker, M.-C. Chen, and V. V. Galy
595 (2018), Microbial oxidation of lithospheric organic carbon in rapidly eroding tropical mountain soils, Science,
596 360(6385), 209-212, doi:10.1126/science.aao6463.
597 Hilton, R.G., Galy, A., Hovius, N., Chen, M.-C., Horng, M.-J., Chen, H., 2008. Tropical-cyclone-driven erosion of
598 the terrestrial biosphere from mountains. Nature Geoscience 1, 759-762.
599 Hilton, R. G., and A. J. West (2020), Mountains, erosion and the carbon cycle, *Nature Reviews Earth &*
600 *Environment*, *1*(6), 284-299.
601 Hilton, R. G. (2016), Climate regulates the erosional carbon export from the terrestrial biosphere, Geomorphology,
602 doi:10.1016/j.geomorph.2016.03.028.
603 Hilton, R. G., J. Gaillardet, D. Calmels, and J.-L. Birck (2014), Geological respiration of a mountain belt revealed
604 by the trace element rhenium, Earth and Planetary Science Letters, 403, 27-36, doi:10.1016/j.epsl.2014.06.021.
605 Hilton, R. G., A. Galy, N. Hovius, M.-J. Horng, and H. Chen (2010), The isotopic composition of particulate organic
606 carbon in mountain rivers of Taiwan, Geochimica et Cosmochimica Acta, 74(11), 3164-3181,
607 doi:10.1016/j.gca.2010.03.004.
608 Hilton, R. G., A. Galy, N. Hovius, and M. J. Horng (2011), Efficient transport of fossil organic carbon to the ocean
609 by steep mountain rivers: an orogenic carbon sequestration mechanism, Geology, 39, 71-74.
610 Hilton, R. G., A. Galy, N. Hovius, S.-J. Kao, M.-J. Horng, and H. Chen (2012), Climatic and geomorphic controls
611 on the erosion of terrestrial biomass from subtropical mountain forest, Global Biogeochemical Cycles, 26(3),
612 n/a-n/a, doi:10.1029/2012gb004314.
613 Ho, C.-S. (1988), An introduction to the geology of Taiwan, explanatory text of the geologic map of Taiwan,
614 *Central Geological Survey*, 151-152.
615 Horan, K., R. G. Hilton, M. Dellinger, E. Tipper, V. Galy, D. Calmels, D. Selby, J. Gaillardet, C. J. Ottley, and D. R.
616 Parsons (2019), Carbon dioxide emissions by rock organic carbon oxidation and the net geochemical carbon
617 budget of the Mackenzie River Basin, American Journal of Science, 319(6), 473-499.
618 Horan, K., R. G. Hilton, D. Selby, C. J. Ottley, D. R. Gröcke, M. Hicks, and K. W. Burton (2017), Mountain
619 glaciation drives rapid oxidation of rock-bound organic carbon, Science Advances, 3(10), e1701107.
620 Hsieh, M.-L., L. S.-H. Lai, C. D.-J. Lin, and J. B. H. Shyu (2012), Late Quaternary landscape evolution and genesis
621 of the 2009 catastrophic landslide in the Hsiao-lin area, southwestern Taiwan, *Geomorphology*, *179*, 225-239,
622 doi:10.1016/j.geomorph.2012.08.014.
623 Hsieh, M.-L., K.-E. Ching, S.-J. Chyi, S.-C. Kang, and C.-Y. Chou (2014), Late Quaternary mass-wasting records in
624 the actively uplifting Pa-chang catchment, southwestern Taiwan, *Geomorphology*, *216*, 125-140,
625 doi:10.1016/j.geomorph.2014.03.040.
626 Huang, Y. H., Hung, C. Y., Lin, I. R., Kume, T., Menyailo, O. V., & Cheng, C. H. (2017). Soil respiration patterns
627 and rates at three Taiwanese forest plantations: dependence on elevation, temperature, precipitation, and
628 litterfall. Bot Stud, 58(1), 49.
629 Kao, S.J., Liu, K.K., 1996, Particulate organic carbon export from a subtropical mountainous river (Lanyang Hsi) in
630 Taiwan. Limnology and Oceanography 41, 1749-1757.
631 Kao, S., M. Dai, K. Wei, N. Blair, and W. Lyons (2008), Enhanced supply of fossil organic carbon to the Okinawa
632 Trough since the last deglaciation, Paleoceanography, 23(2).
633 Kao, S., & Milliman, J. (2008). Water and sediment discharge from small mountainous rivers, Taiwan: The roles of
634 lithology, episodic events, and human activities. The Journal of geology, 116(5), 431-448.
635 Kao, S. J., et al. (2014), Preservation of terrestrial organic carbon in marine sediments offshore Taiwan: mountain
636 building and atmospheric carbon dioxide sequestration, Earth Surface Dynamics, 2(1), 127-139,
637 doi:10.5194/esurf-2-127-2014.
638 Lee, T. Y., J. C. Huang, J. Y. Lee, S. H. Jien, F. Zehetner, and S. J. Kao (2015), Magnified Sediment Export of
639 Small Mountainous Rivers in Taiwan: Chain Reactions from Increased Rainfall Intensity under Global
640 Warming, PloS one, 10(9), e0138283, doi:10.1371/journal.pone.0138283.

Li, H.-C., Liew, P.-M., Seki, O., Kuo, T.-S., Kawamura, K., Wang, L.-C., & Lee, T.-Q. (2013). Paleoclimate variability in central Taiwan during the past 30Kyrs reflected by pollen, δ13CTOC, and n-alkane-δD records in a peat sequence from Toushe Basin. Journal of Asian Earth Sciences, 69, 166-176.

Liew, P., C. Kuo, S. Huang, and M. Tseng (1998), Vegetation change and terrestrial carbon storage in eastern Asia during the Last Glacial Maximum as indicated by a new pollen record from central Taiwan, *Global and Planetary Change*, *16*, 85-94.

Liew, P.-M., S.-Y. Huang, and C.-M. J. Q. I. Kuo (2006), Pollen stratigraphy, vegetation and environment of the last glacial and Holocene—a record from Toushe Basin, central Taiwan, *Quaternary International***,** *147*(1), 16-33.

Lin, B., Liu, Z., Eglinton, T. I., Kandasamy, S., Blattmann, T. M., Haghipour, N., et al. (2020). Island-wide variation in provenance of riverine sedimentary organic carbon: A case study from Taiwan. Earth and Planetary Science Letters, 539.

Lloyd, J., & Taylor, J. (1994). On the temperature dependence of soil respiration. *Functional Ecology*, 315-323.

Lyons, S. L., Baczynski, A. A., Babila, T. L., Bralower, T. J., Hajek, E. A., Kump, L. R., et al. (2018). Palaeocene–Eocene Thermal Maximum prolonged by fossil carbon oxidation. *Nature Geoscience, 12*(1), 54-60.

McLennan, S. M. (1993). Weathering and global denudation. *The Journal of geology, 101*(2), 295-303.

Melillo, J., Steudler, P., Aber, J., Newkirk, K., Lux, H., Bowles, F., et al. (2002). Soil warming and carbon-cycle feedbacks to the climate system. *Science, 298*(5601), 2173-2176.

Milliman, J., Lee, T., Huang, J., & Kao, S. J (2017). Impact of catastrophic events on small mountainous rivers: Temporal and spatial variations in suspended-and dissolved-solid fluxes along the Choshui River, central western Taiwan, during typhoon Mindulle, July 2–6, 2004. *Geochimica et Cosmochimica Acta,* 205, 272-294.

O'Gorman, P. A., R. P. Allan, M. P. Byrne, and M. Previdi (2012), Energetic constraints on precipitation under climate change, Surveys in geophysics, 33(3-4), 585-608.

Roylands, T., Hilton, R. G., Garnett, M. H., Soulet, G., Newton, J.-A., Peterkin, J. L., & Hancock, P. (2022). Capturing the short-term variability of carbon dioxide emissions from sedimentary rock weathering in a remote mountainous catchment, New Zealand. *Chemical Geology, 608*, 121024.

Sarmiento, J., Sundquist, E., 1992, Revised budget for the oceanic uptake of anthropogenic carbon dioxide, *Nature, 356*(6370), 589-593.

Soulet, G., Hilton, R. G., Garnett, M. H., Roylands, T., Klotz, S., Croissant, T., et al. (2021). Temperature control on CO2 emissions from the weathering of sedimentary rocks. *Nature Geoscience, 14*(9), 665-671.

Stallard, R.F., 1998, Terrestrial sedimentation and the carbon cycle: coupling weathering and erosion to carbon burial, Global Biogeochemical Cycles 12, 231-257.

Sundquist, E.T., and Visser, K., 2004, The geologic history of the carbon cycle, in Schlesinger, W.H., ed., Treatise on Geochemistry, Volume 8, Bio- geochemistry: Oxford, UK, Elsevier-Pergamon, p. 425–472.

Tsui, C.-C., Tsai, C.-C., & Chen, Z.-S. (2013). Soil organic carbon stocks in relation to elevation gradients in volcanic ash soils of Taiwan. Geoderma, 209, 119-127.

Tune, A. K., Druhan, J. L., Lawrence, C. R., & Rempe, D. M. (2023). Deep root activity overprints weathering of petrogenic organic carbon in shale. *Earth and Planetary Science Letters, 607*, 118048.

Wang, H. C., K. C. Lin, and C. y. Huang (2016), Temporal and spatial patterns of remotely sensed litterfall in tropical and subtropical forests of Taiwan, *Journal of Geophysical Research: Biogeosciences*, *121*(2), 509-522.

Wang, Y. J., H. Cheng, R. L. Edwards, Z. S. An, J. Y. Wu, C. C. Shen, and J. A. Dorale (2001), A high-resolution absolute-dated late Pleistocene Monsoon record from Hulu Cave, China, *Science*, 294(5550), 2345-2348, doi:10.1126/science.1064618.

Yang, T.-N., T.-Q. Lee, P. A. Meyers, S.-R. Song, S.-J. Kao, L. Löwemark, R.-F. Chen, H.-F. Chen, K.-Y. Wei, and C.-W. Fan (2011), Variations in monsoonal rainfall over the last 21 kyr inferred from sedimentary organic matter in Tung-Yuan Pond, southern Taiwan, *Quaternary Science Reviews*, *30*(23-24), 3413-3422.

Yang, R. J., J. T. Liu, D. Fan, G. S. Burr, H.-L. Lin, and T.-T. Chen (2017), Land-sea duel in the late Quaternary at the mouth of a small river with high sediment yield, Journal of Asian Earth Sciences, 143, 59-76, doi:10.1016/j.jseaes.2017.03.028.

Yu, S.-W., L. L. Tsai, P. J. Talling, A. T. Lin, H.-S. Mii, S.-H. Chung, and C.-S. Horng (2017), Sea level and climatic controls on turbidite occurrence for the past 26 kyr on the flank of the Gaoping Canyon off SW Taiwan, *Marine Geology*, *392*, 140-150, doi:10.1016/j.margeo.2017.0

Zhao, Y., Yang, S., Liu, J. T., Fan, D., Yang, R. J., Bi, L., & Chang, Y.-p. (2017). Reconstruction of silicate weathering intensity and paleoenvironmental change during the late Quaternary in the Zhuoshui River catchment in Taiwan. *Quaternary International , 452*, 43-53.

695 Zheng, L.-W., Ding, X., Liu, J. T., Li, D., Lee, T.-Y., Zheng, X., et al. (2017). Isotopic evidence for the influence of
696 typhoons and submarine canyons on the sourcing and transport behavior of biospheric organic carbon to the
697 deep sea. *Earth and Planetary Science Letters, 465*, 103-111.